

## Proline 107 Is a Major Determinant in Maintaining the Structure of the Distal Pocket and Reactivity of the High-Spin Heme of MauG

Manliang Feng,<sup>†</sup> Lyndal M. R. Jensen,<sup>‡</sup> Erik T. Yukl,<sup>‡</sup> Xiaoxi Wei,<sup>§</sup> Aimin Liu,<sup>§</sup> Carrie M. Wilmot,<sup>‡</sup> and Victor L. Davidson<sup>\*||</sup>

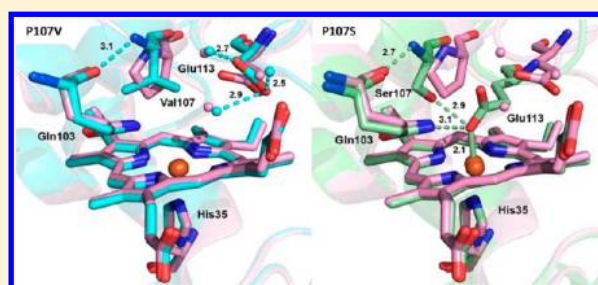
<sup>†</sup>Department of Chemistry, Tougaloo College, Tougaloo, Mississippi 39174, United States

<sup>‡</sup>Department of Biochemistry, Molecular Biology and Biophysics, University of Minnesota, Minneapolis, Minnesota 55455, United States

<sup>§</sup>Department of Chemistry, Georgia State University, P.O. Box 4098, Atlanta, Georgia 30303, United States

<sup>||</sup>Burnett School of Biomedical Sciences, College of Medicine, University of Central Florida, Orlando, Florida 32827, United States

**ABSTRACT:** The diheme enzyme MauG catalyzes a six-electron oxidation required for posttranslational modification of a precursor of methylamine dehydrogenase (preMADH) to complete the biosynthesis of its protein-derived tryptophan tryptophylquinone (TTQ) cofactor. Crystallographic studies had shown that Pro107, which resides in the distal pocket of the high-spin heme of MauG, changes conformation upon binding of CO or NO to the heme iron. In this study, Pro107 was converted to Cys, Val, and Ser by site-directed mutagenesis. The structures of each of these MauG mutant proteins in complex with preMADH were determined, as were their physical and catalytic properties. P107C MauG was inactive, and the crystal structure revealed that Cys107 had been oxidatively modified to a sulfinic acid. Mass spectrometry revealed that this modification was present prior to crystallization. P107V MauG exhibited spectroscopic and catalytic properties that were similar to those of wild-type MauG, but P107V MauG was more susceptible to oxidative damage. The P107S mutation caused a structural change that resulted in the five-coordinate high-spin heme being converted to a six-coordinate heme with a distal axial ligand provided by Glu113. EPR and resonance Raman spectroscopy revealed this heme remained high-spin but with greatly increased rhombicity as compared to that of the axial signal of wild-type MauG. P107S MauG was resistant to reduction by dithionite and reaction with H<sub>2</sub>O<sub>2</sub> and unable to catalyze TTQ biosynthesis. These results show that the presence of Pro107 is critical in maintaining the proper structure of the distal heme pocket of the high-spin heme of MauG, allowing exogenous ligands to bind and directing the reactivity of the heme-activated oxygen during catalysis, thus minimizing the oxidation of other residues of MauG.



MauG is a di-*c*-type heme enzyme<sup>1</sup> responsible for the posttranslational modification of methylamine dehydrogenase (MADH)<sup>2</sup> that generates the protein-derived cofactor,<sup>2–4</sup> tryptophan tryptophylquinone (TTQ).<sup>5</sup> In MADH from *Paracoccus denitrificans*, TTQ is formed from residues  $\beta$ Trp57 and  $\beta$ Trp108.<sup>6</sup> The substrate for this reaction is a monohydroxylated precursor (preMADH) in which one oxygen atom has been inserted into the indole ring of  $\beta$ Trp57.<sup>7,8</sup> Maturation of the TTQ cofactor is a six-electron oxidation process comprised of three two-electron oxidations: insertion of the second OH group into  $\beta$ Trp57, formation of the cross-link between  $\beta$ Trp57 and  $\beta$ Trp108, and oxidation of the quinol to quinone. These two-electron oxidation reactions require the formation of a high-valent bis-Fe(IV) MauG intermediate<sup>9</sup> in which one heme is present as Fe(IV)=O with an axial ligand provided by a His and the other is present as Fe(IV) with His-Tyr axial ligation and no exogenous ligand. This redox state is stabilized even though the two heme irons are separated by 21.1 Å.

The crystal structure of MauG in complex with preMADH<sup>10</sup> revealed that the residues that are modified to form TTQ do not make direct contact with either heme of MauG, and

therefore, the biosynthetic redox reactions within the protein complex require long-range electron transfer. The shortest distance between  $\beta$ Trp108 of preMADH and the iron of the oxygen-binding five-coordinate heme is 40.1 Å, and the shortest distance to the iron of the six-coordinate heme is 19.4 Å. The crystallized complex is catalytically active as it was demonstrated that addition of H<sub>2</sub>O<sub>2</sub> to the protein crystal resulted in formation of mature TTQ within preMADH.<sup>10</sup> Recently, mutation of Trp199 of MauG, which resides at the MauG–preMADH interface, revealed that a hopping mechanism of electron transfer via this residue was required for MauG-dependent biosynthesis of TTQ from preMADH.<sup>11</sup>

The crystal structure of the MauG–preMADH complex also revealed interesting features of the two heme sites. As stated earlier, the six-coordinate heme exhibits His-Tyr ligation, which is unique for a *c*-type heme. This inspired a subsequent study

Received: December 19, 2011

Revised: February 1, 2012

Published: February 2, 2012



that showed that mutation of the ligand Tyr294 to His led to a His-His ligated heme and abolished TTQ biosynthesis in preMADH.<sup>12</sup> Rather than stabilizing a bis-Fe(IV) state, Y294H MauG formed a compound I-like intermediate. It was concluded that this was not sufficient to support biosynthesis because the required electron transfer was now from preMADH to the five-coordinate heme iron (40.1 Å) rather than the closer six-coordinate heme iron (19.4 Å).

A noteworthy feature of the open distal heme pocket at the high-spin heme site was the presence of residue Pro107. A functional role for this residue was implied by the crystal structures of CO and NO adducts of MauG in complex with preMADH.<sup>13</sup> Pro107 displayed movement when going from the diferrrous to the NO- and CO-bound states. Proline side chains can adopt two different conformational states that differ by the sign of their dihedral angles.<sup>14</sup> Binding of CO or NO converted Pro107 from one conformation to the other, and it was suggested that this conversion represented a mechanism for relieving steric crowding by Pro107. It was also noted that Pro107 might play a steric role in O<sub>2</sub> activation by positioning the distal oxygen atom near the carboxylate of Glu113, which is also perturbed by ligand binding.

In this study, Pro107 was mutated to Cys, Val, and Ser. These mutations each had different effects on the structure of the heme site, the spectroscopic properties, and the reactivity of the hemes. These results describe how Pro107 is critical in maintaining the structure of the distal heme pocket of the five-coordinate heme for proper ligand binding and reactivity.

## MATERIALS AND METHODS

**Protein Expression and Purification.** Recombinant MauG<sup>1</sup> and MADH<sup>15</sup> were purified from *P. denitrificans* as described previously. PreMADH<sup>16</sup> was expressed in *Rhodobacter sphaeroides* and purified as described previously.<sup>17</sup> Pro107 of MauG was converted to Ser, Val, and Cys by site-directed mutagenesis of double-stranded pMEG391,<sup>1</sup> which contains *mauG*, using the Phusion site-directed mutagenesis kit. Mutant MauGs were expressed in *P. denitrificans* and isolated from the periplasmic fraction as described for recombinant wild-type (WT) MauG.<sup>1</sup>

**Mass Spectrometry.** Pro107 mutant MauG proteins were subjected to analysis by mass spectrometry. Samples were desalted and exchanged into a 75:25 acetonitrile/water mixture with 0.1% formic acid using C4 resin ZipTip pipet tips (Millipore) prior to introduction into the mass spectrometer. Data were acquired on a QSTAR XL (AB Sciex) quadrupole time-of-flight mass spectrometer with the IonSpray electrospray source. Samples were manually injected into a 10 μL sample loop plumbed into the divert/inject valve of the instrument. Samples were infused at a flow rate of 10 μL/min with a 50:50 acetonitrile/water mixture with 0.1% formic acid. The IonSpray voltage was 4700 V. The TOF region acceleration voltage was 4 kV, and the injection pulse repetition rate was 4.9 kHz. The monoisotopic peaks of the human renin substrate tetradecapeptide from Sigma-Aldrich (St. Louis, MO) were used for external calibration ([M + 3H]<sup>3+</sup> at 586.9830 and [M + 2H]<sup>2+</sup> at 879.9705). TOF MS spectra were acquired from *m/z* 700 to 2200 for approximately 5 min with a 1 s accumulation time. The acquisition software was Analyst QS version 1.0 (AB Sciex). The Bayesian protein reconstruct tool in BioAnalyst extensions version 1.1 (AB Sciex) was used for multiple-charge-state data deconvolution of the intact proteins.

**Crystallization and X-ray Structure Determinations of the P107S, -V, and -C MauG–PreMADH Complexes.** A 2:1 Pro107 mutant MauG/preMADH mixture corresponding to the stoichiometry observed in the WT MauG–preMADH molecular complex was used. These protein complexes crystallized through optimization of the conditions previously established for the WT MauG–preMADH complex<sup>10</sup> by hanging drop vapor diffusion in VDX plates (Hampton Research). Single crystals suitable for X-ray data collection were obtained from drops assembled with 1 μL of the protein solution layered with 3 μL of the reservoir solution over a 22–26% (w/v) PEG 8000, 0.1 M sodium acetate, 0.1 M MES (pH 6.4) reservoir. Crystals were cryoprotected as described previously through the inclusion of 10% PEG 400.<sup>10</sup> X-ray diffraction data were collected at GM/CA-CAT beamlines 23-ID-B and 23-ID-D of the Advanced Photon Source (APS, Argonne National Laboratory, Argonne, IL). Data were collected at 100 K using a beam size matching the dimensions of the largest crystal face. The diffraction data are in space group *P1* with one complex (two P107S, -V, or -C MauG molecules bound to one preMADH molecule) in the asymmetric unit. The data were processed with HKL2000.<sup>18</sup>

Although the space groups of the mutants were triclinic, they were in two different crystal forms distinct from the WT MauG–preMADH *P1* crystal form. The P107V and P107S MauG–preMADH complexes were isomorphous with each other, but the P107C MauG–preMADH complex had a different *P1* cell. Thus, structure solutions were obtained by molecular replacement using PHASER<sup>19</sup> from the CCP4 program suite<sup>20</sup> with the entire WT complex [Protein Data Bank (PDB) entry 3L4M] as the search model. Refinement was conducted using REFMAC<sup>21</sup> in the CCP4 program suite,<sup>20</sup> and model building was conducted in COOT.<sup>22</sup> Restrained refinement with TLS was conducted using no distance restraints between the heme iron centers and their ligands. Residue 107 of each MauG mutant was well-ordered and added to the model based on the  $2F_o - F_c$  and  $F_o - F_c$  electron density maps. Refinement was assessed as complete when the  $F_o - F_c$  electron density contained only noise.

**EPR Spectroscopy.** EPR samples were prepared in 50 mM potassium phosphate buffer (pH 7.4) with 150 μM WT, P107S, or P107V MauG. Continuous wave X-band EPR spectra were recorded on a Bruker E200 spectrometer at a 100 kHz modulation frequency using a dual mode resonator. The temperature was maintained at 10 K with an ESR910 liquid helium cryostat and an ITC503 temperature controller.

**Resonance Raman Spectroscopy.** Resonance Raman spectra were recorded at 25 °C using a Raman spectrometer consisting of a Spex model 1877 triple spectrograph and a CCD detector as reported previously.<sup>23</sup> A 406.7 nm line from an argon–krypton ion laser (Spectra-Physics BeamLok model 2080-KV) was used as the excitation source, and the Raman signal was collected in a 120° geometry. The laser power was adjusted to ~5 mW at the sample. Each spectrum was recorded with a 60 s accumulation time, and 10 repetitively measured spectra were averaged to improve the quality of the final spectrum. The frequencies of the Raman bands were calibrated using the standard spectra of cyclohexane.

**Spectrophotometric Assay of TTQ Biosynthesis in Vitro.** Steady-state spectrophotometric assays of MauG-dependent TTQ biosynthesis, using preMADH as a substrate, were performed as described previously.<sup>24</sup> The standard assay contained 0.3 μM MauG and varied concentrations of

Table 1. X-ray Crystallography Data Collection and Refinement Statistics

	P107V MauG–preMADH	P107S MauG–preMADH	P107C MauG–preMADH
Data Collection			
space group	P1	P1	P1
unit cell lengths (Å)	55.6, 89.0, 104.8	55.6, 89.0, 104.8	55.9, 88.5, 107.7
unit cell angles (deg)	67.1, 79.5, 79.7	67.1, 79.5, 79.7	116.2, 91.8, 99.4
wavelength (Å)	1.03320	1.03320	1.03320
resolution (Å) <sup>a</sup>	50.00–1.87 (1.90–1.87)	50.00–1.63 (1.66–1.63)	50.00–2.52 (2.56–2.52)
no. of measured reflections	349049	771620	127662
no. of unique reflections	145458	208546	61043
completeness (%) <sup>a</sup>	97.0 (86.4)	92.4 (58.6)	97.2 (94.9)
R <sub>merge</sub> (%) <sup>a,b</sup>	3.9 (11.8)	5.1 (29.2)	6.2 (24.1)
I/σI <sup>a</sup>	21.1 (7.7)	24.2 (2.9)	13.8 (3.4)
multiplicity <sup>a</sup>	2.4 (2.3)	3.7 (2.6)	2.2 (2.1)
Refinement			
resolution (Å) <sup>a</sup>	33.89–1.86 (1.91–1.86)	29.39–1.63 (1.67–1.63)	47.86–2.52 (2.59–2.52)
no. of reflections (working/test)	138130/7327	198077/10468	56313/2992
R <sub>work</sub> (%) <sup>c</sup>	13.1	14.2	17.4
R <sub>free</sub> (%) <sup>d</sup>	17.4	18.0	24.3
no. of protein atoms	13179	13106	13356
no. of ligand atoms	237	223	198
no. of solvent sites	2107	1966	388
Ramachandran statistics <sup>e</sup>			
allowed (%)	99.16	99.09	99.11
outliers (%)	0.84	0.91	0.89
root-mean-square deviation			
bond lengths (Å)	0.025	0.028	0.016
bond angles (deg)	2.09	2.35	1.56
average B factor (Å <sup>2</sup> )	19.37	22.23	52.77
ESU (Å) <sup>f</sup> , R <sub>work</sub> /R <sub>free</sub>	null/0.113	null/0.085	2.287/0.314
PDB entry	3SVW	3SJL	3SLE

<sup>a</sup>Values in parentheses are for the highest-resolution shell. <sup>b</sup>R<sub>merge</sub> =  $\sum_i |I_{hkl,i} - \langle I_{hkl} \rangle| / \sum_{hkl} \sum_p I_{hkl,p}$ , where  $I$  is the observed intensity and  $\langle I_{hkl} \rangle$  is the average intensity of multiple measurements. <sup>c</sup>R<sub>work</sub> =  $\sum ||F_o| - |F_c|| / \sum |F_o|$ , where  $F_o$  is the observed structure factor amplitude and  $F_c$  is the calculated structure factor amplitude. <sup>d</sup>R<sub>free</sub> is the R factor based on 5% of the data excluded from refinement. <sup>e</sup>Based on values attained from refinement validation options in COOT. <sup>f</sup>Estimated standard uncertainties generated for R<sub>work</sub> and R<sub>free</sub> in Refmac version 5.5 in the CCP4i suite.

preMADH in 0.01 M potassium phosphate buffer (pH 7.5). The reaction was initiated by the addition of 0.1 mM H<sub>2</sub>O<sub>2</sub>. TTQ biosynthesis was monitored by the increase in absorbance at 440 nm, and the data were fit to eq 1.

$$v/E = k_{\text{cat}}[S]/([S] + K_m) \quad (1)$$

## RESULTS AND DISCUSSION

**Crystal Structures of the P107 Mutant MauG–preMADH Complexes.** Each of the mutant complexes crystallized in space group P1 with two MauG molecules bound to a single preMADH tetramer in the asymmetric unit. The P107V, P107S, and P107C MauG–preMADH crystal structures were determined to 1.86, 1.63, and 2.5 Å resolution, respectively. Although all three mutant structures are in different crystal forms with respect to that of the WT MauG–preMADH crystals, the overall structures are nearly identical to the WT structure with a root-mean-square deviation of 0.22–0.35 Å, the largest deviation belonging to the lower-resolution P107C MauG–preMADH structure. Data collection and refinement statistics are listed in Table 1.

Analysis of the P107V MauG–preMADH structure demonstrates that substitution of Pro with Val at position 107 has very little impact on the organization of the high-spin heme distal pocket (Figures 1A and 2A). Val107 occupies a position very similar to that of Pro in the WT structure, and the positions of

distal water molecules are conserved, although the mutation causes a modest repositioning of Glu113.

In the P107S MauG–preMADH structure, Glu113 has moved 3.1 Å into the distal pocket to coordinate the heme iron at an Fe–O distance of 2.1 Å (Figures 1B and 2B). The movement of Glu113 disrupts a hydrogen bond between the backbone carbonyl of this residue and the backbone amide of Asp57 (Figure 1C). Asp57 is in a large loop stretching from Ala40 to Tyr72 in the WT structure. In the P107S MauG–preMADH structure, residues 49–62 could not be modeled in either MauG chain, suggesting that this region is disordered in the mutant structure. One of the P107V MauG chains can be modeled in this region, although the temperature factors are relatively high. This suggests that the higher level of disorder of this region in P107S MauG cannot be solely attributed to the change in the crystal form of these two mutants compared to WT but is at least partially due to the ligation of Glu113 to the heme iron. While not naturally occurring but a result of the P107S mutation, this structure represents a rare example of axial ligation of a protein-bound heme by a Glu. Another example is a cytochrome *c* peroxidase in which the proximal His ligand has been mutated to Glu.<sup>25,26</sup> This differs from P107S MauG in that the proximal His ligand remains unchanged and the Glu ligand is introduced at the distal site as a consequence of a mutation-induced conformational change. Axial coordination of a Glu to a heme has also been proposed for the

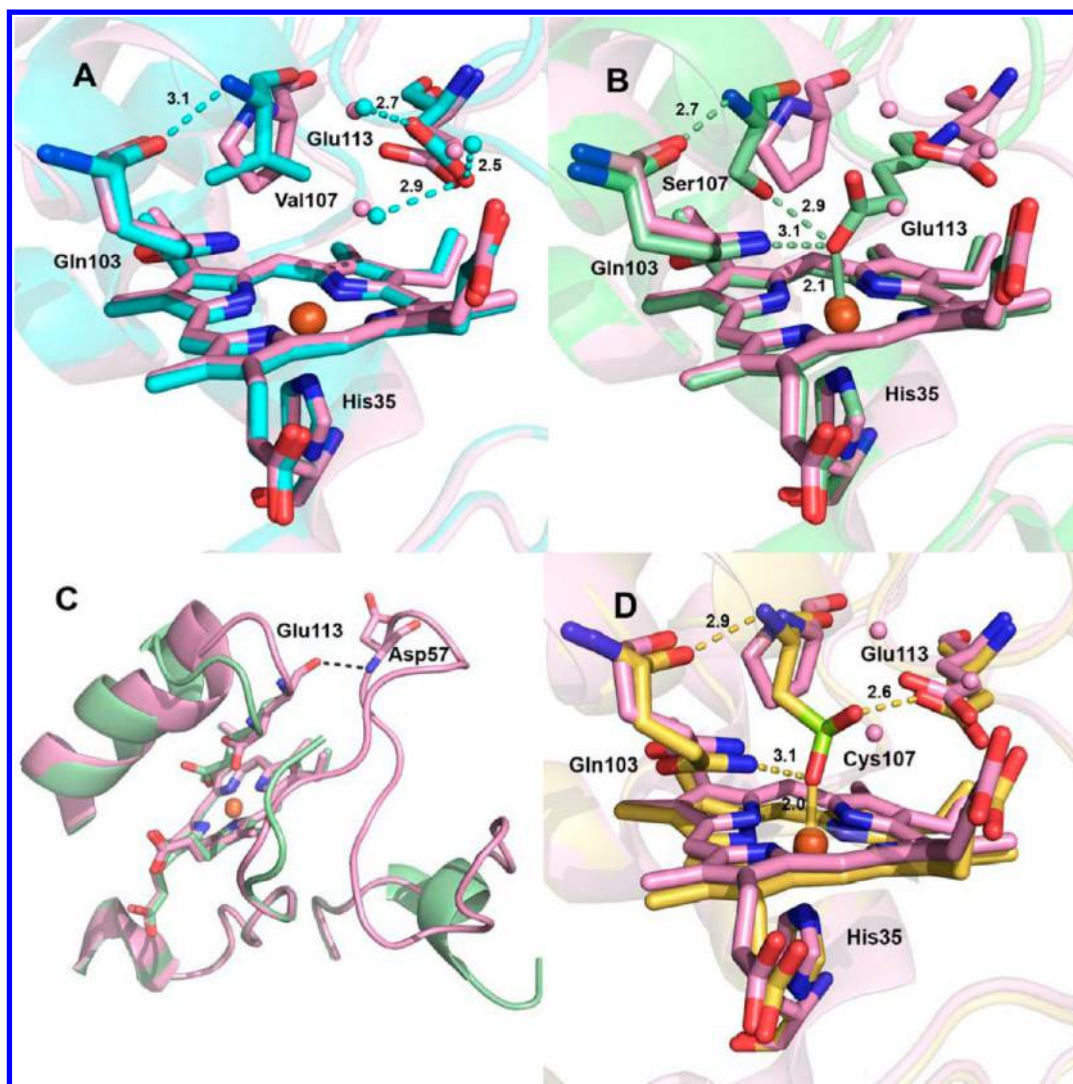


**Figure 1.** High-spin heme environment of (A) P107V (cyan) and (B) P107S (green) MauG vs WT MauG (pink, PDB entry 3L4M) in complex with preMADH. (C) Destabilization of a loop structure in P107S MauG (green) vs WT MauG (pink) in complex with preMADH. (D) High-spin heme environment of P107C MauG (yellow) vs WT MauG (pink) in complex with preMADH. Hemes and residues of interest are drawn as sticks colored by atom, with the remaining protein shown as a cartoon. The iron is displayed as an orange sphere. Hydrogen bonds are shown as dashed lines. This figure was produced using PyMOL (<http://www.pymol.org/>).

cytochrome maturation protein CcmE on the basis of EPR spectroscopy.<sup>27</sup>

In the P107C MauG–preMADH structure, refinement of a Cys residue at position 107 resulted in significant positive difference density between it and the heme iron. To obtain a satisfactory fit to the density, a cysteine-derived sulfenic acid residue was built at this position (Figures 1D and 2C). The modified residue appears to be coordinating the heme iron through an oxygen atom at a distance of 2.0 Å. Mass spectrometry of P107C MauG confirms that prior to crystallization a +32 mass shift from the predicted mass was present, indicating that cysteine modification is not an artifact of radiation damage. This oxidatively modified residue in the proximity of the oxygen-binding heme illustrates how reactive the intermediates are in the normal catalytic process, and that oxidative damage can occur when the MauG distal pocket structure is perturbed.

**Effects of Mutation of Pro107 on MauG-Dependent TTQ Biosynthesis from PreMADH.** The enzymatic activity of Pro107 mutant MauGs was assayed in a steady-state assay of TTQ biosynthesis with preMADH as the substrate and 0.1 mM

H<sub>2</sub>O<sub>2</sub> as the source of oxidizing equivalents. The kinetic parameters for the reaction with P107V MauG were similar to those reported for WT MauG in the steady-state assay with H<sub>2</sub>O<sub>2</sub>.<sup>28</sup> A comparison is shown in Figure 3, where P107V MauG exhibited a  $k_{\text{cat}}$  of  $0.10 \pm 0.01 \text{ s}^{-1}$  and a  $K_{\text{m}}$  of  $1.3 \pm 0.1 \mu\text{M}$  and WT MauG exhibited a  $k_{\text{cat}}$  of  $0.16 \pm 0.02 \text{ s}^{-1}$  and a  $K_{\text{m}}$  of  $1.7 \pm 0.4 \mu\text{M}$  (Figure 3). In contrast, under these experimental conditions, P107S MauG exhibited no TTQ biosynthesis activity. For P107C MauG, the ready oxidation of Cys107 to sulfenic acid during overexpression and purification, both of which are performed under aerobic conditions, led to batch-to-batch variation in activity. This ranged from no activity to activity that was quickly lost, even during storage at  $-80 \text{ }^{\circ}\text{C}$ . Given the inability to obtain a homogeneous preparation of the unmodified P107C variant, further investigation of the properties of the Pro107 mutants focused on characterization of P107V MauG and P107S MauG.

**Effects of Mutation of Pro107 on the Absorption Spectrum of MauG and Reactivity toward Dithionite and H<sub>2</sub>O<sub>2</sub>.** The P107V and P107S mutations each had a

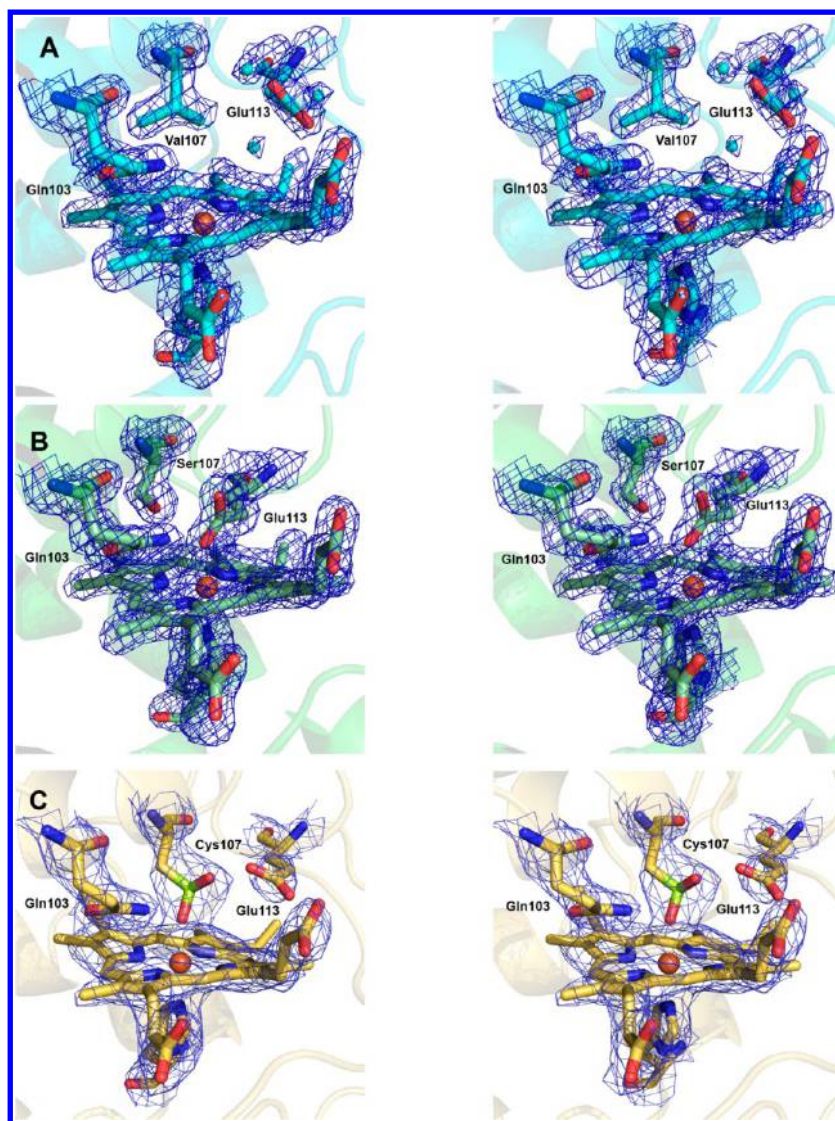


**Figure 2.** Stereoviews of electron density for the high-spin heme environment of (A) P107V (cyan), (B) P107S (green), and (C) P107C (yellow) MauG in complex with preMADH. The  $2F_o - F_c$  electron density is shown as blue mesh contoured to  $1.5\sigma$ . Hemes and residues of interest are drawn as sticks colored by atom, with the remaining protein shown as a cartoon. The iron is displayed as an orange sphere. This figure was produced using PyMOL (<http://www.pymol.org/>).

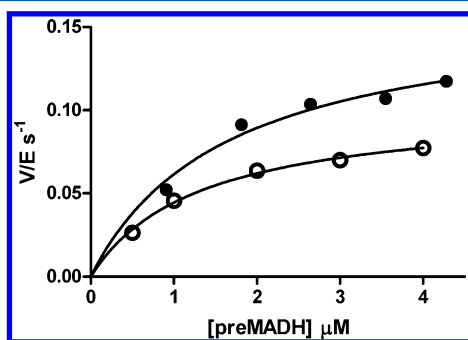


**Figure 3.** Steady-state kinetic analysis of P107V MauG-dependent TTQ biosynthesis from preMADH. Data are shown for the reactions catalyzed by P107V MauG (○) and WT MauG (●). The lines are fits of the data by eq 1.

different effect on the absorption spectrum of the diferric protein (Figure 4). The spectrum of P107V MauG is similar to that of WT MauG in that the Soret peak is centered at 406 nm. However, the Soret peak of P107V MauG is much broader. For

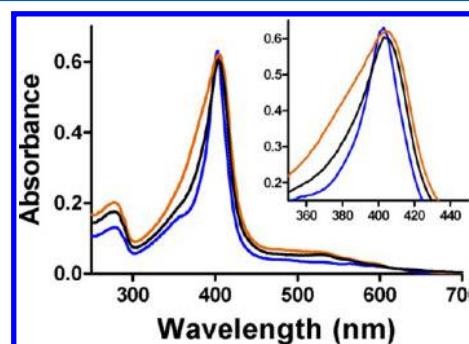


**Figure 4.** Visible absorption spectra of WT MauG and P107 MauG mutants. Overlay of the absorption spectra of WT MauG (black), P107V MauG (brown), and P107S MauG (blue). The overlay of the Soret peak region of each spectrum is magnified in the inset.

P107S MauG, the Soret peak is centered at 403 nm and is narrower than that of WT MauG.

The P107V and P107S mutations also each differentially affected the ability to generate the diferric state of the protein.

Reduction of WT MauG is characterized by the red shift of the Soret peak to 418 nm and the appearance of relatively sharp  $\alpha$  and  $\beta$  bands at 550 and 520 nm, respectively. The reductive titration of WT MauG with dithionite requires 2 equiv of electrons, and reaction with dithionite is very rapid. In contrast, P107S MauG did not react at all after addition of a stoichiometric amount of dithionite. To obtain a spectrum similar to that of diferric WT MauG, the addition of 20 equiv of dithionite was required and took 30 min to complete the spectral change. When the protein was treated with excess ferricyanide to reoxidize the protein, it was not possible to regenerate the spectrum of the as-isolated diferric protein, indicating that the protein was likely damaged because of the harsher conditions required for reduction. This was also the case for P107V MauG; however, the process required addition of a smaller excess of dithionite, and the rate of reduction was much faster. This suggests that displacement of the heme-ligated Glu113 in the P107S mutant is a significant factor in the time taken to achieve reduction, but the damage is primarily the result of requiring a stoichiometric excess of reducing equivalents for reduction, which does occur in both P107S and P107V MauG. Unfortunately, the inability to achieve efficient reversible reduction of these MauG mutant proteins precluded the possibility of determining the redox potentials for the diferric/diferrous couple.

Reaction of WT MauG with  $\text{H}_2\text{O}_2$  yields a high-valent bis-Fe(IV) species that is evidenced by the decreased intensity and red shift of the Soret peak. The bis-Fe(IV) species forms rapidly (within 2 ms) after addition of a stoichiometric amount of  $\text{H}_2\text{O}_2$  to diferric MauG. In the absence of the preMADH substrate, this high-valent species spontaneously returns to the diferric form in  $\sim 10$  min. P107V MauG similarly reacts with  $\text{H}_2\text{O}_2$  rapidly to yield similar spectral changes and shows a spontaneous return to diferric protein with a slight increase in the absorbance of the Soret peak. In contrast, addition of a stoichiometric amount of  $\text{H}_2\text{O}_2$  to P107S MauG did not cause the spectrum to change. Only when a very large excess of  $\text{H}_2\text{O}_2$  was added was a spectral change observed; however, it was not characteristic of bis-Fe(IV). Instead, a very slow decrease of the absorbance of the Soret peak with no concomitant red shift was observed, and the species that was formed did not spontaneously return to the initial state. This suggests the need to displace the iron-ligated Glu113 may be impeding the reaction with  $\text{H}_2\text{O}_2$ , as discussed above for the dithionite reduction. The inability of P107S MauG to react with  $\text{H}_2\text{O}_2$  also provides an explanation for the inability to catalyze TTQ biosynthesis.

**Effects of Mutation of Pro107 on the EPR Spectrum of MauG.** The low-temperature X-band EPR spectrum of WT MauG exhibits signals from three ferric heme species. A low-spin ( $S = 1/2$ ) heme with  $g$  values of 1.87, 2.19, and 2.54, assigned to the His-Tyr-ligated heme, accounts for  $\sim 50\%$  of the total signal. A high-spin ( $S = 5/2$ ) heme with  $g$  values of 1.99 and 5.57, assigned to the five-coordinate His-ligated heme, accounts for  $\sim 25\%$  of the total signal. A second broad low-spin heme with  $g$  values of 1.52, 2.32, and 2.89 is observed and accounts for the remaining 25%. This species has been assigned as a freezing artifact that is derived from approximately half of the high-spin heme upon freezing.<sup>10</sup> Whereas the EPR spectrum of diferric P107V MauG presented high- and low-spin heme signals very similar to those observed in the WT MauG spectrum, the EPR spectrum of P107S MauG exhibited features quite different from those of WT MauG (Figure 5). The high-spin ferric signal at a  $g$  value of 5.57 in P107S MauG appears to

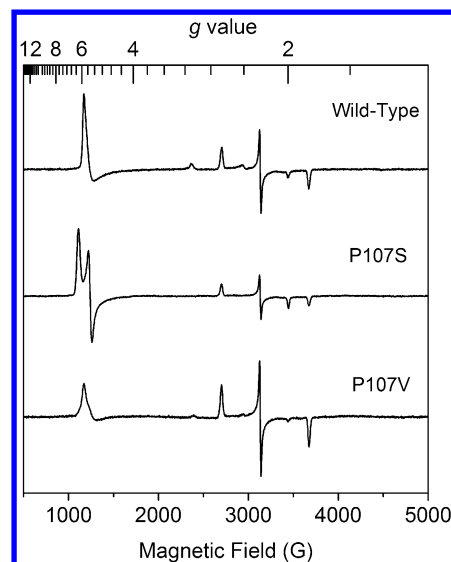


**Figure 5.** EPR spectra of WT MauG (top), P107S MauG (middle) and P107V MauG (bottom). EPR parameters for obtaining spectra were as follows: temperature, 10 K; microwave power, 1 mW at 9.44 GHz; modulation amplitude, 0.5 mT.

be split into two signals. This feature reflects a much increased rhombicity as compared to the axial signal of WT MauG. The resolved  $g$  values for the high-spin ferric heme are as follows:  $g_x = 1.99$ ,  $g_y = 5.55$ , and  $g_z = 6.21$ . The low-spin ferric signal assigned to the His-Tyr-ligated heme remained the same as seen in WT MauG.

Such an increased rhombicity, as is seen for the high-spin heme in P107S MauG, is typically caused by addition of one or more ligands and is consistent with the crystal structure of the P107S MauG–preMADH complex that shows monodentate distal ligation by Glu113. Glutamate is considered a weak ligand for a heme iron, and EPR shows the heme remains high-spin even with the Fe–O distance of 2.1 Å seen in the crystal structure. The broad low-spin ferric EPR signal with a  $g_{\text{max}}$  of 2.89 that was assigned as a freezing artifact in WT MauG is completely absent in the spectrum of P107S MauG. The conversion of high-spin to low-spin heme upon freezing is well-documented in diheme enzymes, with some cases leading to complete loss of the high-spin ferric signal.<sup>29–32</sup> The absence of the freezing artifact in P107S MauG is consistent with a sixth ligand that is difficult to displace and prevents coordination by a stronger internal ligand following a freezing-induced structural change.

**Effects of Mutation of Pro107 on the Resonance Raman Spectra of MauG.** The resonance Raman spectrum of P107V MauG is similar to that of native MauG, indicating that this mutation does not induce a significant structural change in the hemes. In contrast, the resonance Raman spectrum of P107S MauG revealed frequency changes in several of the marker bands relative to WT MauG, indicating a significant change in the heme structure that is consistent with ligation of Glu113 to the heme. The high-frequency region of the spectra (Figure 6A) contains several marker bands that are sensitive to oxidation state, spin state, and the conformation of the heme macrocycle.<sup>33–35</sup> The assignment of marker bands is based on the work of Spiro and co-workers.<sup>34</sup> The  $\nu_2$  and  $\nu_3$  bands of P107S MauG at 1567 and 1472  $\text{cm}^{-1}$ , respectively, are from high-spin heme, consistent with the presence of high-spin heme in the EPR spectrum. These  $\nu_2$  and  $\nu_3$  bands are also shifted to

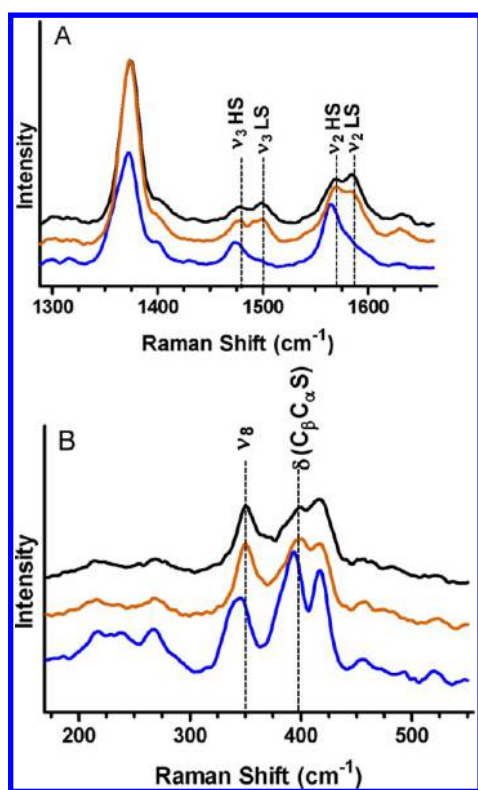


**Figure 6.** Resonance Raman spectrum of WT MauG and Pro107 MauG mutants. Overlay of the spectra of diferric WT MauG (black), P107V MauG (brown), and P107S MauG (blue) in the high-frequency (A) and low-frequency (B) regions. Relevant marker bands are indicated.

lower frequencies compared with the frequencies of the corresponding high-spin marker bands of WT MauG (1571 and 1478  $\text{cm}^{-1}$ , respectively). The frequencies of the  $\nu_2$  and  $\nu_3$  bands from the low-spin heme, which are somewhat obscured by the high-spin bands, are basically unchanged from those of WT MauG. In the low-frequency region (Figure 6B), the  $\delta$  ( $\text{C}_\beta\text{C}_\alpha\text{S}$ ) mode is shifted from 393  $\text{cm}^{-1}$  in WT MauG to 390  $\text{cm}^{-1}$  in P107S MauG. The  $\nu_8$  mode is also shifted to a lower frequency compared to that of WT MauG. These shifts suggest conformational changes resulting in the thioether bonds to the heme becoming more restrained.

**Effects of Mutation of Pro107 on the Susceptibility of MauG to Oxidative Damage.** It was previously shown that WT MauG is inactivated when supplied with oxidation equivalents in the absence of preMADH.<sup>36</sup> As discussed above, Cys107 in P107C MauG was oxidized to a sulfinic acid, as evidenced by the crystal structure and analysis by mass spectrometry. As such, it was of interest to determine whether the P107V and P107S mutations might also make MauG more susceptible to oxidative damage. To test this, 20  $\mu\text{M}$  MauG was incubated in the presence of 200  $\mu\text{M}$   $\text{H}_2\text{O}_2$  for 1 h before the reaction was quenched by the addition of a small amount of catalase. Each sample was then subjected to ESI-MS (Figure 7). The pattern of oxidation products is different among WT and mutant proteins. WT MauG forms predominantly a single oxidation product with the very slow buildup of a second product. In P107V MauG, at least three oxidized species are formed, and in P107S MauG, there appear to be no fewer than six formed with complete loss of the parent peak during the 1 h incubation time. As discussed earlier, P107S MauG is unreactive toward

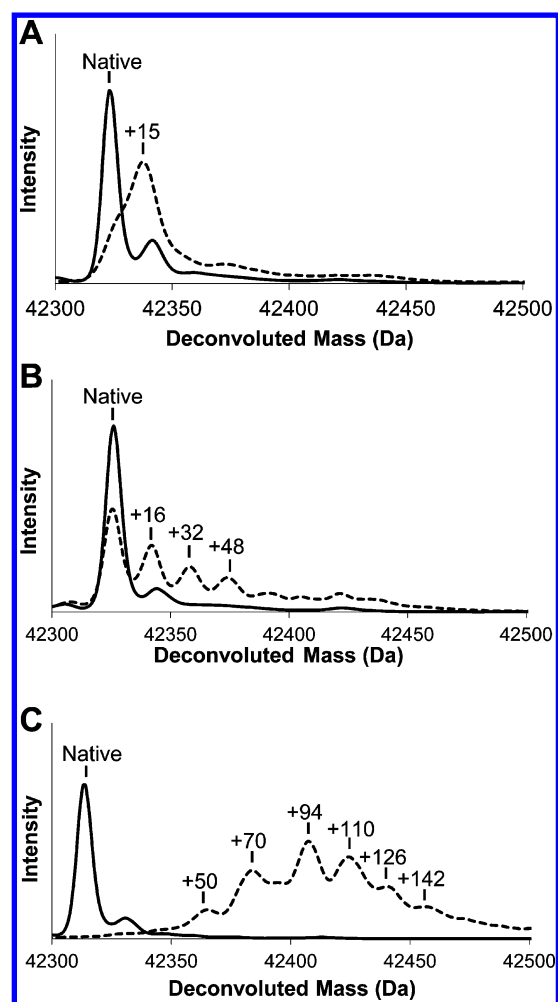


**Figure 7.** Deconvoluted mass spectra of 20  $\mu\text{M}$  WT (A), P107V (B), and P107S (C) MauG before (—) and after (---) treatment with 200  $\mu\text{M}$   $\text{H}_2\text{O}_2$  for 1 h.

stoichiometric  $\text{H}_2\text{O}_2$  and exhibits an irreversible decrease in absorbance of the Soret peak upon addition of excess  $\text{H}_2\text{O}_2$ . The mass spectrometry data indicate that those  $\text{H}_2\text{O}_2$ -induced spectral changes are likely associated with  $\text{H}_2\text{O}_2$ -induced oxidative damage. Thus, each of the mutations of Pro107 makes MauG much more susceptible to oxidative damage.

**Conclusions.** The results of this study clearly show that the presence of Pro107 is critical in maintaining the proper structure of the distal heme pocket of the high-spin heme of MauG. The structural role of Pro107 seems in large part to be a feature of its size rather than rigidity because P107V MauG reacts with  $\text{H}_2\text{O}_2$  and exhibits reasonable TTQ biosynthesis activity. However, P107V MauG is more susceptible to oxidative damage than WT MauG. Oxidative damage is also observed for P107C MauG in which Cys107 becomes oxidized to a sulfinic acid. The altered structural and physical properties of P107S MauG demonstrate that Pro107 is important not only for maintaining an open site at the high-spin heme iron to allow binding of exogenous ligands and reactants, including  $\text{H}_2\text{O}_2$ , but also for controlling the reactivity of the activated oxygen so that it is used for long-range catalysis, while minimizing oxidation of other residues of MauG. Additionally, P107S MauG results in an unusual structure of a protein-bound heme that is six-coordinate and high-spin with His-Glu axial ligation and unusual spectroscopic properties.

## ■ ASSOCIATED CONTENT

### Accession Codes

Coordinates and structure factors have been deposited as Protein Data Bank entries 3SVW (P107V MauG–preMADH), 3SJL (P107S MauG–preMADH), and 3SLE (P107C MauG–preMADH).

## ■ AUTHOR INFORMATION

### Corresponding Author

\*Burnett School of Biomedical Sciences, College of Medicine, University of Central Florida, 6900 Lake Nona Blvd., Orlando, FL 32827. Telephone: (407) 266-7111. Fax: (407) 266-7002. E-mail: victor.davidson@ucf.edu.

### Author Contributions

L.M.R.J. and E.T.Y. contributed equally to this work.

### Funding

This work was supported by National Science Foundation Grant MCB-0843537 (A.L.), National Institutes of Health Grants GM-41574 (V.L.D.), GM-66569 (C.M.W.), and GM-97779 (E.T.Y.), and Minnesota Partnership for Biotechnology and Medical Genomics Grant SPAP-05-0013-P-FY06 (C.M.W.).

### Notes

The authors declare no competing financial interest.

## ■ ACKNOWLEDGMENTS

We thank Professor Hiroyasu Tachikawa for access to the facilities at Jackson State University for resonance Raman studies, Dr. Sheeyong Lee for his participation in the early stages of these studies, Dr. Sooim Shin for helpful discussion, and Yu Tang for technical assistance. Computer resources were provided by the Basic Sciences Computing Laboratory of the University of Minnesota Supercomputing Institute, and we thank Can Ergenekan for his support. X-ray data were collected at the Kahlert Structural Biology Laboratory (KSBL) at the University of Minnesota and GM/CA-CAT at the Advanced Photon Source (APS). GM/CA CAT has been funded in whole or in part with federal funds from the National Cancer Institute (Y1-CO-1020) and the National Institute of General Medical Sciences (Y1-GM-1104). Use of the Advanced Photon Source was supported by the U.S. Department of Energy, Basic Energy Sciences, Office of Science, under Contract DE-AC02-06CH11357. We thank Ed Hoeffner for KSBL support and the staff at Sector 23, APS, for their support.

## ■ ABBREVIATIONS

MADH, methylamine dehydrogenase; TTQ, tryptophan tryptophylquinone; preMADH, biosynthetic precursor protein of MADH with incompletely synthesized TTQ; bis-Fe(IV) MauG, redox state of MauG with one heme as Fe(IV)=O and the other as Fe(IV); WT, wild-type.

## ■ REFERENCES

- (1) Wang, Y., Graichen, M. E., Liu, A., Pearson, A. R., Wilmot, C. M., and Davidson, V. L. (2003) MauG, a novel diheme protein required for tryptophan tryptophylquinone biogenesis. *Biochemistry* 42, 7318–7325.
- (2) Davidson, V. L. (2001) Pyrroloquinoline quinone (PQQ) from methanol dehydrogenase and tryptophan tryptophylquinone (TTQ) from methylamine dehydrogenase. *Adv. Protein Chem.* 58, 95–140.
- (3) Davidson, V. L. (2007) Protein-derived cofactors. Expanding the scope of post-translational modifications. *Biochemistry* 46, 5283–5292.

- (4) Davidson, V. L. (2011) Generation of protein-derived redox cofactors by posttranslational modification. *Mol. Biosyst.* 7, 29–37.
- (5) McIntire, W. S., Wemmer, D. E., Chistoserdov, A., and Lidstrom, M. E. (1991) A new cofactor in a prokaryotic enzyme: Tryptophan tryptophylquinone as the redox prosthetic group in methylamine dehydrogenase. *Science* 252, 817–824.
- (6) Chen, L., Doi, M., Durley, R. C., Chistoserdov, A. Y., Lidstrom, M. E., Davidson, V. L., and Mathews, F. S. (1998) Refined crystal structure of methylamine dehydrogenase from *Paracoccus denitrificans* at 1.75 Å resolution. *J. Mol. Biol.* 276, 131–149.
- (7) Pearson, A. R., De La Mora-Rey, T., Graichen, M. E., Wang, Y., Jones, L. H., Marimanikkupam, S., Aggar, S. A., Grimsrud, P. A., Davidson, V. L., and Wilmot, C. M. (2004) Further insights into quinone cofactor biogenesis: Probing the role of mauG in methylamine dehydrogenase tryptophan tryptophylquinone formation. *Biochemistry* 43, 5494–5502.
- (8) Wang, Y., Li, X., Jones, L. H., Pearson, A. R., Wilmot, C. M., and Davidson, V. L. (2005) MauG-dependent in vitro biosynthesis of tryptophan tryptophylquinone in methylamine dehydrogenase. *J. Am. Chem. Soc.* 127, 8258–8259.
- (9) Li, X., Fu, R., Lee, S., Krebs, C., Davidson, V. L., and Liu, A. (2008) A catalytic di-heme bis-Fe(IV) intermediate, alternative to an Fe(IV)=O porphyrin radical. *Proc. Natl. Acad. Sci. U.S.A.* 105, 8597–8600.
- (10) Jensen, L. M., Sanishvili, R., Davidson, V. L., and Wilmot, C. M. (2010) In crystallo posttranslational modification within a MauG/pre-methylamine dehydrogenase complex. *Science* 327, 1392–1394.
- (11) Abu Tarboush, N., Jensen, L. M. R., Yukl, E. T., Geng, J., Liu, A., Wilmot, C. M., and Davidson, V. L. (2011) Mutagenesis of tryptophan199 suggests that hopping is required for MauG-dependent tryptophan tryptophylquinone biosynthesis. *Proc. Natl. Acad. Sci. U.S.A.* 108, 16956–16961.
- (12) Abu Tarboush, N., Jensen, L. M., Feng, M., Tachikawa, H., Wilmot, C. M., and Davidson, V. L. (2010) Functional importance of tyrosine 294 and the catalytic selectivity for the bis-Fe(IV) state of MauG revealed by replacement of this axial heme ligand with histidine. *Biochemistry* 49, 9783–9791.
- (13) Yukl, E. T., Goblirsch, B. R., Davidson, V. L., and Wilmot, C. M. (2011) Crystal structures of CO and NO adducts of MauG in complex with pre-methylamine dehydrogenase: Implications for the mechanism of dioxygen activation. *Biochemistry* 50, 2931–2938.
- (14) Nemethy, G., Gibson, K. D., Palmer, K. A., Yoon, C. N., Paterlini, G., Zagari, A., Rumsey, S., and Scheraga, H. A. (1992) Energy parameters in polypeptides. 10. Improved geometrical parameters and nonbonded interactions for use in the ECEPP/3 algorithm, with application to proline-containing peptides. *J. Phys. Chem.* 96, 6472–6484.
- (15) Davidson, V. L. (1990) Methylamine dehydrogenases from methylotrophic bacteria. *Methods Enzymol.* 188, 241–246.
- (16) Pearson, A. R., de la Mora-Rey, T., Graichen, M. E., Wang, Y., Jones, L. H., Marimanikkupam, S., Aggar, S. A., Grimsrud, P. A., Davidson, V. L., and Wilmot, C. W. (2004) Further insights into quinone cofactor biogenesis: Probing the role of MauG in methylamine dehydrogenase TTQ formation. *Biochemistry* 43, 5494–5502.
- (17) Graichen, M. E., Jones, L. H., Sharma, B. V., van Spanning, R. J., Hosler, J. P., and Davidson, V. L. (1999) Heterologous expression of correctly assembled methylamine dehydrogenase in *Rhodobacter sphaeroides*. *J. Bacteriol.* 181, 4216–4222.
- (18) Otwinowski, Z., and Minor, W. (1997) Processing of X-ray diffraction data collected in oscillation mode. *Methods Enzymol.* 276, 307–326.
- (19) McCoy, A. J., Grosse-Kunstleve, R. W., Adams, P. D., Winn, M. D., Storoni, L. C., and Read, R. J. (2007) Phaser crystallographic software. *J. Appl. Crystallogr.* 40, 658–674.
- (20) Collaborative Computational Project Number 4 (1994) The CCP4 suite: Programs for protein crystallography. *Acta Crystallogr. D50*, 760–763.
- (21) Murshudov, G. N., Vagin, A. A., and Dodson, E. J. (1997) Refinement of macromolecular structures by the maximum-likelihood method. *Acta Crystallogr. D53*, 240–255.

(22) Emsley, P., and Cowtan, K. (2004) Coot: Model-building tools for molecular graphics. *Acta Crystallogr. D60*, 2126–2132.

(23) Li, X., Feng, M., Wang, Y., Tachikawa, H., and Davidson, V. L. (2006) Evidence for redox cooperativity between *c*-type hemes of MauG which is likely coupled to oxygen activation during tryptophan tryptophylquinone biosynthesis. *Biochemistry* 45, 821–828.

(24) Li, X., Jones, L. H., Pearson, A. R., Wilmot, C. M., and Davidson, V. L. (2006) Mechanistic possibilities in MauG-dependent tryptophan tryptophylquinone biosynthesis. *Biochemistry* 45, 13276–13283.

(25) Choudhury, K., Sundaramoorthy, M., Hickman, A., Yonetani, T., Woehl, E., Dunn, M. F., and Poulos, T. L. (1994) Role of the proximal ligand in peroxidase catalysis: Crystallographic, kinetic, and spectral studies of cytochrome-*c* peroxidase proximal ligand mutants. *J. Biol. Chem.* 269, 20239–20249.

(26) Smulevich, G., Neri, F., Willemsen, O., Choudhury, K., Marzocchi, M. P., and Poulos, T. L. (1995) Effect of the His175-Glu mutation on the heme pocket architecture of cytochrome-*c* peroxidase. *Biochemistry* 34, 13485–13490.

(27) Garcia-Rubio, I., Braun, M., Gromov, I., Thony-Meyer, L., and Schweiger, A. (2007) Axial coordination of heme in ferric CcmE chaperone characterized by EPR spectroscopy. *Biophys. J.* 92, 1361–1373.

(28) Shin, S., Feng, M. L., Chen, Y., Jensen, L. M. R., Tachikawa, H., Wilmot, C. M., Liu, A., and Davidson, V. L. (2011) The tightly bound calcium of MauG is required for tryptophan tryptophylquinone cofactor biosynthesis. *Biochemistry* 50, 144–150.

(29) Fulop, V., Watmouth, N. J., and Ferguson, S. J. (2001) Structure and enzymology of two bacterial diheme enzymes: Cytochrome *cd*<sub>1</sub> nitrite reductase and cytochrome *c* peroxidase. *Adv. Inorg. Chem.* 51, 163–204.

(30) Arciero, D. M., and Hooper, A. B. (1994) A di-heme cytochrome-*c* peroxidase from *Nitrosomonas europaea* catalytically active in both the oxidized and half-reduced states. *J. Biol. Chem.* 269, 11878–11886.

(31) Foote, N., Peterson, J., Gadsby, P. M. A., Greenwood, C., and Thomson, A. J. (1985) Redox-linked spin-state changes in the di-heme cytochrome *c*-551 peroxidase from *Pseudomonas aeruginosa*. *Biochem. J.* 230, 227–237.

(32) Prazeres, S., Moura, J. J. G., Moura, I., Gilmour, R., Goodhew, C. F., Pettigrew, G. W., Ravi, N., and Huynh, B. H. (1995) Mössbauer characterization of *Paracoccus denitrificans* cytochrome-*c* peroxidase. Further evidence for redox and calcium binding-induced heme-heme interaction. *J. Biol. Chem.* 270, 24264–24269.

(33) Desbois, A. (1994) Resonance Raman spectroscopy of *c*-type cytochromes. *Biochimie* 76, 693–707.

(34) Hu, S., Morris, I. K., Singh, J. P., Smith, K. M., and Spiro, T. G. (1993) Complete assignment of cytochrome *c* resonance Raman spectra via enzymatic reconstitution, with isotopically labelled hemes. *J. Am. Chem. Soc.* 115, 12446–12458.

(35) Tu, A. T. (1982) *Raman spectroscopy in biology; principles and applications*, pp 331–337, John Wiley and Sons Inc., New York.

(36) Shin, S., Lee, S., and Davidson, V. L. (2009) Suicide inactivation of MauG during reaction with O<sub>2</sub> or H<sub>2</sub>O<sub>2</sub> in the absence of its natural protein substrate. *Biochemistry* 48, 10106–10112.